Density Functional Theory Integrated with Renormalization Group Theory for Criticality of Nanoconfined Fluids

Ming Zeng, Jianguo Mi,* and Chongli Zhong

Laboratory of Computational Chemistry, Department of Chemical Engineering Beijing University of Chemical Technology, Beijing 100029, China

Received: November 21, 2009; Revised Manuscript Received: February 3, 2010

Nanoconfined fluids exhibit complicated behavior such as phase transitions, prewetting, wetting transitions, universal critical properties, and critical point shifts, attributed to the cooperative interactions of short- and long-range density fluctuations. In this work, a theoretical approach, an integrated density functional (DF) and renormalization group (RG) theory, is developed to investigate the critical properties of fluids confined in slit pores or bounded by single wall surfaces. The approach can take into account both the local and the long-range density fluctuations of confined fluids self-consistently. The predicted critical order parameter exponent β is about $^1/_8$, and the wetting exponent β_s is 1.056 ± 0.011. These values are quite close to the two-dimensional Ising values, demonstrating that the new theoretical approach is reliable as a description of criticality in nanoconfined fluids. Correspondingly, the global phase transitions and surface wetting transitions are analyzed.

1. Introduction

Confined fluids exhibit a variety of properties that differ substantially from those of bulk fluids.[1−7] The phase transitions, surface wetting, wetting transitions, freezing, and critical phenomena are particularly rich,[8−13] because the combined effects of finite-size and specific wall−fluid interactions are pronounced. Investigation of these properties is crucial to syntheses and applications of new nanomaterials. In recent years, great efforts have been made to interpret the physical behavior of confined fluids theoretically; however, it is still a challenge to describe these properties within one theoretical framework.

In the past two decades, the well-known Ising lattice model analysis of critical exponents has seen extensive applications.[14−16] The theory, when applied to describe phase transitions and wetting transitions of nanoconfined fluids, provides only a qualitative description. Recently, the structure and properties of nanoconfined fluids have been extensively investigated by molecular simulation[17−21] and density functional theory.[22−24] Those approaches obtained some success in characterizing first-order layering transition and wetting behavior far from the critical region, but they merely avoided the critical region or failed at and near criticality owing to their intrinsic mean-field nature or as a result of severe and uncorrected finite-size limitations generating mean-field-like results. Very recently, several new computational methods have been successfully developed to deal with singular critical behavior, such as dynamic renormalization,[25] entanglement renormalization,[26] and renormalized multibondic cluster simulations.[27] These works are helpful for understanding the critical properties of confined fluids, but they do not easily cross over consistently from first-order phase transitions to the critical region. Thus, the calculated critical properties are approximate because of the finite lattice choice in the molecular simulations.

In this work, we propose a new way to solve the problem by establishing a theoretical approach that focuses on the essential feature of fluid fluctuations. When the confining walls attract the atoms of a fluid, finite-size contributions to the free energy of the confined fluids give rise to a force between the walls. The force depends on the bulk state point and the wall−fluid potentials, as well as on pore width, and yields local, or short-range, density fluctuations. As the temperature increases up to the critical region, the force becomes long-ranged, resulting in long-range density fluctuations. Thus, the fluid exhibits compositive waves of short and long range. To deal with this complexity, an inhomogeneous theory is necessary and valid only after the long-range density fluctuations are taken fully into account by using some transformation. The best transformation for the abnormal critical fluctuations is renormalization group (RG) theory. This theory, originally proposed by Wilson[28,29] for Ising spins and lattice gases, has become central to any discussion of critical phenomena.

To establish a general theoretical approach for fluids confined to slit pores (i.e., the space between two closely spaced parallel planes), we adopted a new density functional[30] to describe local density fluctuations and developed a new confined RG transformation to deal with long-range density fluctuations. The new RG transformation was developed based on our previous RG theory for bulk fluids.[31,32]

Outside the critical region, where the local density fluctuations are dominant, we used the modified fundamental measure theory (MFMT),[33] which yields very accurate density profiles for hard spheres inside slit pores. For the attractive part, we adopted a free energy functional based on the first-order mean spherical approximation (FMSA) model.[30,34] The free energy was constructed by combining that of the bulk fluid with a weighted density approximation. Instead of using mean-field theory, we applied the direct correlation function (DCF) to determine the weight function. The adopted DCF was refined by solving the Ornstein−Zernike (OZ) integral equation, in which an accurate radial distribution function (RDF) is employed as input.[30] Here, the RDF was originally developed by FMSA and further improved by a simplified exponential approximation. The much improved and explicit RDF and DCF provide an accurate description of the fluid structure, as well as the first-order phase

* Corresponding author. E-mail: mijg@mail.buct.edu.cn.

10.1021/jp911070a
Published on Web 02/25/2010

and wetting transitions. Inside the critical region, the density fluctuations are increasingly long-ranged near the critical point. Unlike bulk fluids, this kind of long-range fluctuation is partly limited because of boundary effects. For fluids confined in a small slit pore, the long-range density fluctuations in the Z direction are confined, and the liquid−vapor critical point belongs to the two-dimensional Ising universality class.[4,6] Hence, the original three-dimensional space waves are limited to two-dimensional plane waves, and the corresponding confined RG transformation has been developed. Most important, we construct our confined RG transformation on the basis of our density functional by sharing the same DCF,[32] which ensures that the theoretical crossover is self-consistent both inside and outside the critical region. The new method is fundamentally rigorous, and to the best of our knowledge, this is the first theoretical approach that can deal accurately with both the outside and the inside of the critical region of nanoconfined fluids.

2. Theory

For simplicity, we explored the phase transition and criticality of Lennard-Jones fluids in an attractive slit pore and the wetting transition on a single wall surface, namely, methane absorbed in slit carbon pores and in a single carbon wall. For methane, treated as a spherical molecule, the interaction between methane molecules is traditionally represented by the Lennard-Jones (LJ) 12−6 potential

$$u^{\mathrm{LJ}}(r) = 4\varepsilon_{\mathrm{ff}}\left[\left(\frac{\sigma_{\mathrm{ff}}}{r}\right)^{12} - \left(\frac{\sigma_{\mathrm{ff}}}{r}\right)^{6}\right] \tag{1}$$

where σ_{ff} is the effective molecular diameter and $\varepsilon_{\mathrm{ff}}$ is the depth of the potential. For methane, parameters from ref 17 were used: $\sigma_{\mathrm{ff}} = 0.373$ nm and $\varepsilon_{\mathrm{ff}}/k_{\mathrm{B}} = 148.1$ K, where k_{B} is the Boltzmann constant.

The interaction between the fluid and the wall is given as

$$V_{\mathrm{s}}(z) = 2\pi\rho_{\mathrm{v}}\varepsilon_{\mathrm{sf}}\sigma_{\mathrm{sf}}{}^{2}\Delta\left[\frac{2}{5}\left(\frac{\sigma_{\mathrm{sf}}}{z}\right)^{10} - \left(\frac{\sigma_{\mathrm{sf}}}{z}\right)^{4} - \frac{\sigma_{\mathrm{sf}}{}^{4}}{3\Delta(0.61 + z)^{3}}\right] \tag{2}$$

in which ρ_{v} is the volume number density of carbon atoms in the wall, with $\rho_{\mathrm{v}} = 114$ nm^{-3}; Δ is the interlayer space, with $\Delta = 0.335$ nm; and σ_{sf} and $\varepsilon_{\mathrm{sf}}$ are the size and energy parameters, respectively, for methane−graphite interactions, with $\sigma_{\mathrm{sf}} = 0.3565$ nm, $\varepsilon_{\mathrm{sf}}/k_{\mathrm{B}} = 21.5$ K for the weak interaction, and $\varepsilon_{\mathrm{sf}}/k_{\mathrm{B}} = 64.5$ K for the strong interaction. The potential field for slit pores includes contributions from two opposing walls: $V_{\mathrm{ext}}(z) = V_{\mathrm{s}}(z) + V_{\mathrm{s}}(H - z)$, where H is the separation between the parallel walls of the slit pore or the layer thickness.

This is a simple system that exhibits the general features of nanoconfined global phase behavior and wetting.

A. Density Functional Theory. For inhomogeneous fluids, the grand potential, $\Omega[\rho(\mathbf{r})]$, can be expressed as the following general form of density functional in terms of the Helmholtz free energy $F[\rho(\mathbf{r})] = \int \mathrm{d}\mathbf{r}\, f[\rho(\mathbf{r})]$, where f is the free energy density, to describe the density profile:

$$\Omega[\rho(\mathbf{r})] = k_{\mathrm{B}}T\int \mathrm{d}\mathbf{r}\, \rho(\mathbf{r})\{\ln[\rho(\mathbf{r})\Lambda^{3}] - 1\} + F_{\mathrm{rep}}[\rho(\mathbf{r})] + F_{\mathrm{att}}[\rho(\mathbf{r})] + \delta F_{\mathrm{RG}}(\rho_{\mathrm{av}}) + \int \mathrm{d}\mathbf{r}\, \{\rho(\mathbf{r})[V_{\mathrm{ext}}(\mathbf{r}) - \mu]\} \tag{3}$$

where T is the absolute temperature, $\rho(\mathbf{r})$ denotes the density distribution for configuration $\mathbf{r}$, $\rho_{\mathrm{av}} = \int_0^H \rho(z)\,\mathrm{d}z/H$ is the average density when considering the confined space with layer thickness H, $F_{\mathrm{rep}}[\rho(\mathbf{r})]$ represents the hard-sphere reference system given by the MFMT, $F_{\mathrm{att}}[\rho(\mathbf{r})]$ accounts for the attractive interactions from the FMSA, and $\delta F_{\mathrm{RG}}(\rho_{\mathrm{av}})$ represents the contribution from the confined RG transform of the long-range density fluctuations. Outside the critical region, $\delta F_{\mathrm{RG}}(\rho_{\mathrm{av}})$ makes no difference, whereas inside the critical region, it is crucial both for second-order phase transitions and critical point calculations. In addition, $V_{\mathrm{ext}}(\mathbf{r})$ is the external potential, and μ is the chemical potential in the ensemble.

According to MFMT,[33] $F_{\mathrm{rep}}[\rho(\mathbf{r})]$ can be represented by

$$F_{\mathrm{rep}}[\rho(\mathbf{r})] = k_{\mathrm{B}}T\int \mathrm{d}\mathbf{r}\left\{-n_0\ln(1 - n_3) + \frac{n_1n_2 - \mathbf{n}_{\mathrm{V1}}\mathbf{n}_{\mathrm{V2}}}{1 - n_3} + \frac{1}{36\pi}\left[n_3\ln(1 - n_3) + \frac{n_3{}^{2}}{(1 - n_3)^{2}}\right]\frac{n_2{}^{3} - 3n_2\mathbf{n}_{\mathrm{V1}}\mathbf{n}_{\mathrm{V2}}}{n_3{}^{3}}\right\} \tag{4}$$

where $\alpha = 0, 1, 2, 3, \mathrm{V1}, \mathrm{V2}$. n_0, n_1, n_2, and n_3 are the scalar-weighted densities, whereas the boldface symbols $\mathbf{n}_{\mathrm{V1}}$ and $\mathbf{n}_{\mathrm{V2}}$ are the vector-weighted densities. They are defined by

$$n_{\alpha}(\mathbf{r}) = \int \rho(\mathbf{r}')\, w^{(\alpha)}(\mathbf{r} - \mathbf{r}')\,\mathrm{d}\mathbf{r}' \tag{5}$$

where the weight functions $w^{(\alpha)}(\mathbf{r})$, $\alpha = 0, 1, 2, 3, \mathrm{V1}, \mathrm{V2}$, are expressed in terms of the Heaviside step function $H(r)$ and the Dirac delta function $\delta(r)$ as

$$w^{(2)}(\mathbf{r}) = \pi d^{2}w^{(0)}(\mathbf{r}) = 2\pi d w^{(1)}(\mathbf{r}) = \delta(d/2 - r) \tag{6}$$

$$w^{(3)}(\mathbf{r}) = H(d/2 - r) \tag{7}$$

$$w^{(\mathrm{V2})}(\mathbf{r}) = 2\pi d w^{(\mathrm{V1})}(\mathbf{r}) = \frac{\mathbf{r}}{r}\delta(d/2 - r) \tag{8}$$

With FMSA and the weighted density approximation,[30] $F_{\mathrm{att}}[\rho(\mathbf{r})]$ can be expressed as

$$F_{\mathrm{att}}[\rho(\mathbf{r})] = \int \rho(\mathbf{r})\, a_{\mathrm{att}}[\bar{\rho}(\mathbf{r})]\,\mathrm{d}\mathbf{r} \tag{9}$$

where $a_{\mathrm{att}} = a_1 + a_2 + a_{\mathrm{r}}$ is the force energy per particle given by combining the FMSA with the simplified exponential approximation.[30] The full, rather complex details are given in the Appendix (see eqs 29−44). $\bar{\rho}(\mathbf{r})$ is the weighted density, given by the weight function $\omega_{\mathrm{att}}(r)$

$$\bar{\rho}(\mathbf{r}) = \int \rho(\mathbf{r}')\, \omega_{\mathrm{att}}(|\mathbf{r} - \mathbf{r}'|)\,\mathrm{d}\mathbf{r}' \tag{10}$$

$$\omega_{\mathrm{att}}(r) = \frac{c_{\mathrm{att}}(r)}{\int c_{\mathrm{att}}(r)\,\mathrm{d}\mathbf{r}} \tag{11}$$

where $c_{\mathrm{att}}(r)$ is the DCF of the bulk fluids from the attractive contribution, and the details are given in the Appendix (see eqs 45−48).

B. Confined Renormalization Group Theory. Following White and Zhang's theory,[35] the long-range density fluctuations can be assumed as

$$\Delta\rho_{\text{fluc}}(\mathbf{r}) = \sqrt{2}x\cos(\mathbf{k}\cdot\mathbf{r}) \tag{12}$$

where x is the fluctuation amplitude and $\mathbf{k}$ is the wave vector. The whole purpose of the RG transform is to incorporate the long-range contribution into the density functional for a strongly inhomogeneous fluid. For confined fluids, the density distribution function $\rho_s(\mathbf{r})$ for a system can be written as[36]

$$\Xi(T,\mu,\Phi) = \sum_{[\rho_s(\mathbf{r})]} \exp\Big\{\beta\mu\int_\Phi d\mathbf{r}\,\rho_s(\mathbf{r}) - \beta\int_\Phi d\mathbf{r}\,f_s[\rho_s(\mathbf{r})] - \beta\int_\Phi d\mathbf{r}\,f_D[\rho_s(\mathbf{r})]\Big\} \tag{13}$$

where $\Xi(T,\mu,\Phi)$ represents the grand canonical partition function of the system within a domain of area $A(\Phi)$ at chemical potential μ. $\rho_s(\mathbf{r})$ is the portion of the whole density $\rho(\mathbf{r})$ with $\lambda > \lambda_s$, whereas those densities with wavelengths $\lambda < \lambda_s$ have been absorbed into the free energy $f_s[\rho_s(\mathbf{r})]$. Note that $f_s[\rho_s(\mathbf{r})]$ is a function, instead of a functional, of $\rho_s(\mathbf{r})$ because of the local nature of this term. $F_D[\rho(\mathbf{r})] = \int d\mathbf{r}\, f_D[\rho(\mathbf{r})]$ represents the nonlocal contribution from density fluctuation[32]

$$\beta F_D[\rho(\mathbf{r})] = -\frac{1}{2}\int c(\mathbf{r}_1-\mathbf{r}_2)\,\Delta\rho(\mathbf{r}_1)\,\Delta\rho(\mathbf{r}_2)\,d\mathbf{r}_1\,d\mathbf{r}_2 + \frac{1}{2}\int c(\mathbf{r}_1-\mathbf{r}_2)\,\delta(\mathbf{r}_1-\mathbf{r}_2)\,\Delta\rho(\mathbf{r}_1)\,\Delta\rho(\mathbf{r}_2)\,d\mathbf{r}_1\,d\mathbf{r}_2 \tag{14}$$

where $c(r)$ is the DCF, which is given in the Appendix, and $\delta(\mathbf{r}_1 - \mathbf{r}_2)$ is the Dirac delta function. Equation 14 indicates that the nonlocal term is the residual of the whole fluctuation contribution after subtraction of the local contribution. The nonlocal contribution is the key issue for fluid critical behavior, and the whole purpose of the RG transform is to absorb this term into the local term. For the selected range of wavelengths $\lambda_s < \lambda < \lambda_1$, such an adsorption results in the expression

$$\Xi(T,\mu,\Phi) = \sum_{[\rho_1(\mathbf{r})]} \exp\Big\{\beta\mu\int_\Phi d\mathbf{r}\,\rho_1(\mathbf{r}) - \beta\int_\Phi d\mathbf{r}\,f_1[\rho_1(\mathbf{r})]\Big\} \tag{15}$$

where $f_1(\rho)$ can be rewritten as a correction to $f_s(\rho)$

$$f_1(\rho) = f_s(\rho) + \delta f_1(\rho) \tag{16}$$

or, more generally, for the nth-step RG correction

$$f_n(\rho) = f_{n-1}(\rho) + \delta f_{\text{RG},n}(\rho), \quad f_0(\rho) = f_{\text{ref}}(\rho) \tag{17}$$

which is the basic recursion equation in the RG theory. In eq 17, ρ is the reference density, which employs the value of the average density, $\rho_{\text{av}} = \int_0^H \rho(z)\,dz/H$, when considering the confined space with layer thickness H. The reference free energy density, f_{ref}, is given by $f_{\text{ref}} = \rho(a_{\text{id}} + a_{\text{hs}} + a_{\text{att}})$. The ideal part of the free energy per particle is $a_{\text{id}} = \ln(\rho\Lambda^3) - 1$, where Λ is the de Broglie wavelength. The hard-sphere contribution to the free energy per particle is $a_{\text{hs}} = (4\eta - 3\eta^2)/[(1-\eta)^2]$, where η is the packing factor ($\eta = {}^1/_6\pi\rho d^3$). The attractive contribution term, a_{att}, is the same as in eq 9. After several transformations[32] of eq 14, adopting a procedure similar to that in White and Zhang's work,[35] we obtain

$$\delta f_{\text{RG},n}(\rho) = -\frac{1}{\beta A_n}\ln\left(\frac{\int_0^\rho dx\exp\{-A_n[\beta f_{n-1,D}(\rho,x) + 2\pi C_{4,\text{att}}x^2k_n^{\,2} - 2\pi C_{6,\text{att}}x^2k_n^{\,4}]\}}{\int_0^\rho dx\exp\{-A_n[\beta f_{n-1,D}(\rho,x) + 2\pi C_{2,\text{att}}x^2]\}}\right) \tag{18}$$

$$f_{n-1,D}(\rho,x) = \frac{f_{n-1}(\rho+x) + f_{n-1}(\rho-x)}{2} - f_{n-1}(\rho) \tag{19}$$

$$C_{n,\text{att}}(r) = \frac{1}{(n-1)!}\int_0^\infty c_{\text{att}}(r)r^n\,d\mathbf{r} \tag{20}$$

The average area of the fluctuation plane, A_n, used in eq 18 is chosen to be a function of wavelength: $A_n = (\lambda_n)^2$, with $\lambda_n = 3^{n-1}\lambda_1$. The initial wavelength λ_1 is assumed to be 4σ. In later transforms, the fluctuation magnitude in the density wave planes is increased by $k_n = k_1/3^{n-1}$, with $k_1 = 2\pi/\lambda_1$.

Combining DFT with the new confined RG transformation, we can calculate the final density distribution by minimizing the grand potential, leading to the result

$$\rho(\mathbf{r}) = \rho\exp\left(\beta\mu - \beta\frac{\delta\{F_{\text{hs}}[\rho(\mathbf{r})] + F_{\text{att}}[\rho(\mathbf{r})]\}}{\delta\rho(\mathbf{r})} - \beta\frac{\delta[\delta F_{\text{RG}}(\rho_{\text{av}})]}{\delta\rho_{\text{av}}} - \beta V_{\text{ext}}(\mathbf{r})\right) \tag{21}$$

where ρ is the bulk density. With eq 21, the local densities $\rho(\mathbf{r})$ can be calculated with an iteration procedure. The initial local density profiles and the average densities can be calculated with the density functional only $\{\delta[\delta F_{\text{RG}}(\rho_{\text{av}})]/\delta\rho_{\text{av}} = 0\}$. Based on the average densities, the confined RG recursions can be performed and added, and the next density profiles are recalculated with the combined DFT and RG. The iterations are performed until the grand potential achieves a minimum.

C. Surface Tension and Wetting Transition. To investigate wetting transition, a surface phase transition from partial to complete wetting, the wetting temperature of the wall, T_w^*, needs to be determined. Young's equation[37] provides a simple description of wetting and drying transitions in terms of the surface tensions of different interfaces. This kind of transition has been studied extensively to evaluate the contact angle for fluid−wall systems[38]

$$\cos\theta = \frac{\gamma_{\text{wl}} - \gamma_{\text{wv}}}{\gamma_{\text{vl}}} \tag{22}$$

where θ is the contact angle and γ_{wl}, γ_{wv}, and γ_{vl} denote the surface tensions of the wall−liquid, wall−vapor, and vapor−liquid interfaces, respectively. For fluid wetting a wall with a given field $V_{\text{ext}}(z)$, γ_{wl}, γ_{wv}, and γ_{vl} are calculated under the bulk coexisting pressure P_{coex} through the equations[39,40]

$$\gamma_{wl,wv} = \int_0^{\infty} \{f[\rho(z)] - \rho(z)\mu_{coex} + \rho(z)\, V_{ext}(z) + P_{coex}\}\, dz \quad (23)$$

and

$$\gamma_{vl} = \int_{\rho_v}^{\rho_l} \{f[\rho(z)] - \rho(z)\mu_{coex} + P_{coex}\}\, dz \quad (24)$$

In eq 23, the density distribution $\rho(z)$ can be calculated with a single wall surface enclosed. In eq 24, the density distribution $\rho(z)$ is determined under the condition that no external field exists. At different temperatures, the contact angle varies from complete drying ($\cos\theta = -1$) to partial wetting ($\cos\theta < 1$) and finally to complete wetting at the wetting temperature T_w at which $\cos\theta = 1$ is first realized.

3. Results and Discussion

To illustrate the above-described procedure, we consider the phase behavior and critical properties of fluids confined in slit pores of different sizes with different attractive fluid−pore wall interactions and wetting behavior of fluids bounded by a single wall surface. As a typical example, we consider methane absorbed in slit carbon pores using the molecular parameters from ref 17.

We start our discussion with the determination of the critical point. For bulk fluids, the critical temperature, $T^*_{c,3D}$, is obtained by minimizing the determinant[41]

$$J = \begin{vmatrix} \frac{\partial x}{\partial \rho} & \frac{\partial x}{\partial T} \\ \frac{\partial y}{\partial \rho} & \frac{\partial y}{\partial T} \end{vmatrix} \quad (25)$$

with

$$x = \left(\frac{\partial P}{\partial \rho}\right)_{T_c}, y = \left(\frac{\partial^2 P}{\partial \rho^2}\right)_{T_c} \quad (26)$$

In contrast, for a confined fluid, the critical temperature T^*_{cp} is very difficult to calculate with eq 25. For simplicity, we determined T^*_{cp} by recognizing that the two equilibrium density profiles, $\rho^*_l(z)$ and $\rho^*_v(z)$ obtained by matching the grand potential become the same, which means that there is no phase transition. The main uncertainty in locating T^*_{cp} comes from the difficulty in distinguishing whether the difference between the equilibrium density profiles disappears. The values of the bulk and confined critical temperatures play a crucial role in determining the critical exponent β, as discussed below.

To determine the phase diagram in a slit pore, it is necessary to obtain the two equilibrium density distributions $\rho^*_v(z)$ and $\rho^*_l(z)$ corresponding to the vapor- and liquid-like phases, respectively. By changing the bulk density ρ^* or the bulk chemical potential μ^*, one can generate a theoretical isotherm that exhibits metastable adsorption and desorption branches of the hysteresis loop, where the stable state is characterized by tracing smaller values of the grand potential. An equilibrium thermodynamic transition can occur between states of equal grand potential. Thus, an intersection on the curve of grand potential density corresponds to the point of an equilibrium transition. This procedure is important to the entire calculation procedure, because it assures thermodynamic consistency with the corresponding bulk fluid.

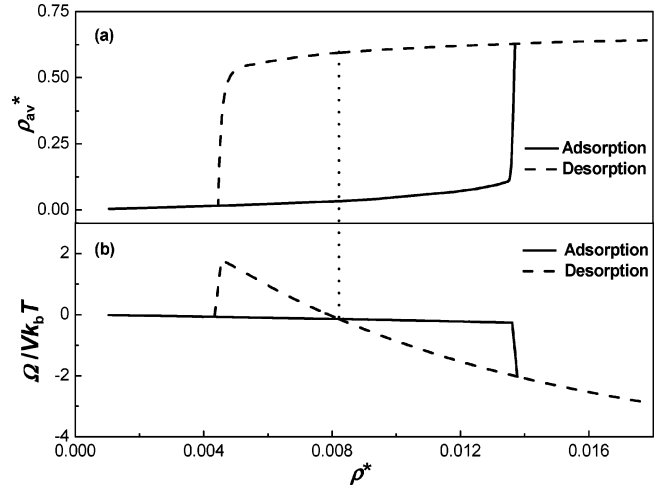

Figure 1. (a) Adsorption isotherm and (b) grand potential density as functions of reduced bulk density in the slit pore ($H = 7.5\sigma$, $\varepsilon_{sf}/k_B = 21.5$ K) at $T^* = 0.850$. The solid and dashed lines represent the results of the adsorption and desorption branches, respectively. The dotted line represents the equilibrium phase transition.

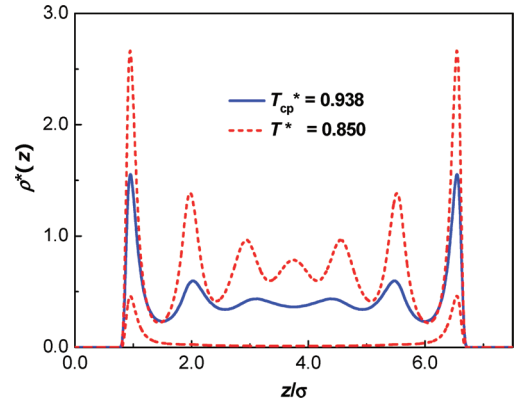

Figure 2. Density profiles with different temperatures at $H = 7.5\sigma$, $\varepsilon_{sf}/k_B = 21.5$ K. Below T^*_{cp}, each temperature has two curves: the upper one is the liquid-like profile, and the lower one is the vapor-like profile.

Figure 1 presents the adsorption isotherm and grand potential density as functions of reduced bulk density for methane in a pore with width $H = 7.5\sigma$ and fluid−solid interaction of strength $\varepsilon_{sf}/k_B = 21.5$ K at reduced temperature $T^* = 0.850$. Focusing on Figure 1b, where the reduced bulk density is smaller than $\rho^* = 0.0082$, the adsorption branch has smaller values, which indicates that the system has a lower energy. However, when the reduced bulk density is greater than $\rho^* = 0.0082$, the desorption branch has the smaller values. Thus, the equilibrium thermodynamic transition occurs at a reduced bulk density of $\rho^* = 0.0082$, the density at which the adsorption and desorption branches cross. The density profiles of these two equilibrium phases at $T^* = 0.850$ and a single density distribution at $T^*_{cp} = 0.938 \pm 0.002$ are plotted in Figure 2. From this figure, one can see that reversible capillary condensation or phase behavior occurs at $T^* < T^*_{cp}$, where T^*_{cp} is the critical temperature of fluids confined in the slit pore. The vapor-like phase at $T^* = 0.850$ consists of a monolayer adsorbed on each side of the wall, whereas the liquid-like phase has more disordered layers in the middle of the pore. Up to the calculated pore critical point (here, $T^*_{cp} = 0.938 \pm 0.002$), there is only one density profile well structured in the direction with respect to the two walls.

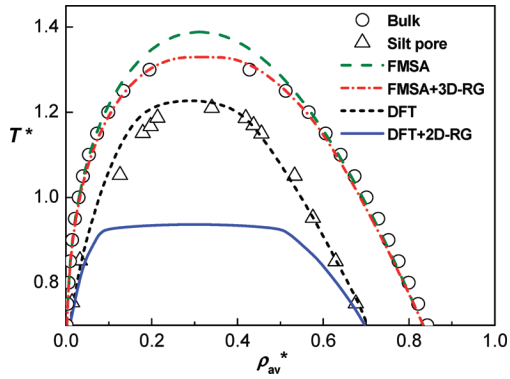

Figure 3. Vapor−liquid phase diagrams predicted by FMSA and FMSA with 3D-RG transformation for bulk fluid and density functional (DF) and DF with 2D-RG transformation for fluid in a slit pore ($H = 7.5\sigma$, $\varepsilon_{sf}/k_B = 21.5$ K). Open circles and triangles represent the molecular simulation data of Lotfi et al.[42] and Vishnyakov et al.,[17] respectively.

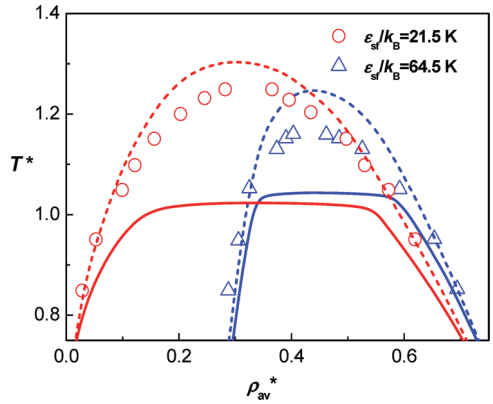

Figure 4. Vapor−liquid phase diagrams in the slit pores predicted by DF (dashed lines) and DF with 2D-RG transformation (solid lines) with different adsorption fields ($H = 10.0\sigma$). The symbols represent molecular simulation data.[17]

With the coexisting density profiles $\rho_l^*(z)$ and $\rho_v^*(z)$ at several different temperatures, the global phase equilibria are investigated by averaging $\rho_l^*(z)$ and $\rho_v^*(z)$ in the Z direction with $\rho_{av}^* = \int_0^H \rho^*(z)\, dz/H$. The predicted phase diagrams from molecular simulation,[17] density functional, and density functional with 2D-RG transform are shown together in Figure 3. For comparison, the simulation data[42] and FMSA with 3D-RG transform for bulk fluids are also included in the figure. Because of the effects of finite size and external field, the critical point of the confined fluid is always lower than that of the bulk fluid. More important, far from the critical point of the confined fluid, one can see that the theoretical results are close to the simulation data and reveal classical first-order phase transitions. The situation also appears in large pores and strong fluid−wall interactions as shown in Figure 4. There are large deviations between the simulation data[17] and the DFT + 2D-RG plots in Figures 3 and 4. This is mainly because the finite size of the basic Monte Carlo cell in the molecular simulations has a significant influence on the critical temperature, and this choice inevitably gives inaccurate results. As the temperature approaches the critical point, the density fluctuations become stronger; hence, the number of particles in the simulation box should have been significantly increased to have sufficiently thick layers of both phases. In contrast, the DFT + 2D-RG model provides a huge convenience to account for these strong density fluctuations and to investigate the critical behavior of confined fluids.

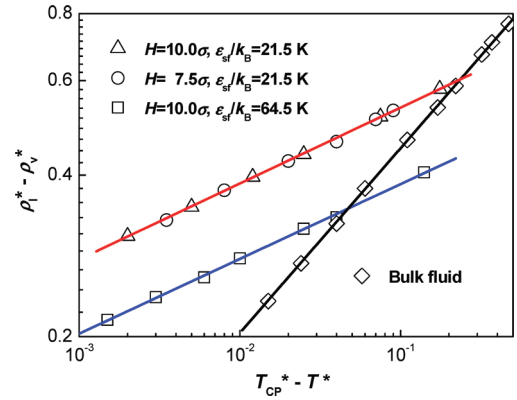

Figure 5. Determination of the critical exponent β. The symbols are calculated results, and the solid lines are the best linear regressions of the symbols.

Summarizing Figures 3 and 4, one can easily determine the critical exponent β using the density order parameter with the scaling law[43]

$$\rho_l^* - \rho_v^* = B(T_c^* - T^*)^\beta \tag{27}$$

where B is an adjustable parameter. Figure 5 presents the density order parameters and the fitting plots, and the slopes of the plots indicate the value of β. For bulk fluid, using our previous three-dimensional RG transform[32] and the equilibrium densities taken from bulk phase diagram calculated by FMSA + 3DRG, we obtain the critical exponent $\beta = 0.334 \pm 0.010$, which is close to numerical estimate of the 3D Ising model $\beta = 0.326$, a typical universal exponent for bulk fluids. In contrast, for fluids confined in small slit pores, β is 0.129 ± 0.007 for strong fluid−wall interactions, and β is 0.127 ± 0.009 for weak fluid−wall interactions. The two values are nearly the same and are very close to the $^1/_8$ of the 2D Ising model. The examination of the critical exponent confirms that the present theory can capture the features of long-range fluctuations in the critical region for confined fluids and correctly describe the second-order phase transitions as well as the critical properties. In contrast, the density functional without RG transform and the simulation[17] yield the mean-field exponent ($\beta \approx 0.5$) and cannot reproduce the second-order phase transitions as well as criticality.

Now, we come to the critical point shifts, which denote the finite-size effects of the slit pores on the critical temperature. When the pore width increases from $H = 7.5\sigma$ to $H = 10.0\sigma$ with a fluid−solid interaction of $\varepsilon_{sf}/k_B = 21.5$ K, the theoretically predicted critical point shifts toward higher temperature (from 0.938 ± 0.002 to 1.024 ± 0.003). An important characteristic of critical point shifts can be tested with the critical wetting exponent β_s, which was originally given by Parry and Evans[44] as

$$T_w^* - T_{cp}^* = H^{-1/\beta_s} \tag{28}$$

where H is the layer thickness and T_w^* can be determined by calculating the contact angle under different temperatures for the given surface fields with eq 22, which is very accurate when used to predict the contact angle in the case of wall−fluid systems.[38] The surface tension γ_{vl} was calculated using a system consisting of a liquid in equilibrium with its vapor, whereas γ_{wl} and γ_{wv} were calculated using the equilibrium liquid and gas chemical potentials, respectively, as reference bulk states

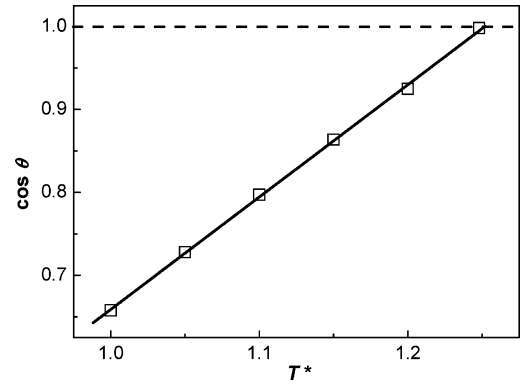

Figure 6. Calculated contact angles as a function of temperature, where the wetting temperature T_w^* corresponds to cos $\theta = 1$. The solid line is a linear fitting of the symbols.

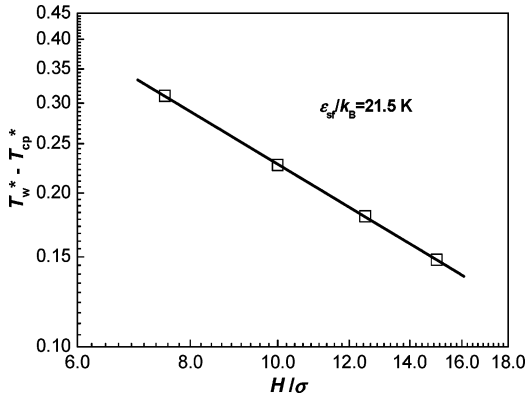

Figure 7. Determination of the critical wetting exponent β_s. The symbols are calculated results, and the solid line is the best linear regression of the symbols.

with a single wall enclosed. Figure 6 presents the variation in wetting angle as the temperature increases. The calculated results can be fitted with a line, showing a distinctive first-order wetting transition. The complete wetting temperature is $T_w^* = 1.248 \pm 0.003$ determined with cos $\theta = 1$, and the corresponding exponent β_s can be derived from Figure 7 with $\beta_s = 1.056 \pm 0.011$, which indeed converges to the exact value[44] $\beta_s = 1$ as the layer thickness H increases. Although the exponent was obtained for a fluid is confined by two parallel walls with different force fields, we believe that it is also suitable for the walls with the same force field when considering the growth of the wetting layer. This gives us some confidence that the present theory should be able to determine the universality of criticality. The exponent also indicates that we cannot recover information about the bulk critical point when the limit $H \rightarrow \infty$ is taken.

4. Conclusions

In summary, a general theory has been developed for fluids confined to slit pores and bounded by single wall surfaces, in which the newly developed density functional part yields reliable predictions of the short-range density fluctuations, fluid structure, and first-order phase and wetting transitions while the newly proposed confined RG transformation part correctly describes the long-range density fluctuations of the critical region, second-order phase transitions, critical point, and critical shifts. In particular, the new theory can cross over from short-range fluctuations to long-range fluctuations consistently. Thus, it can simultaneously capture both the short- and long-range density fluctuations of confined fluids. The phase transitions, wetting transitions, critical point shifts, and critical exponent are correctly predicted. As a result, this work presents a new theory that can contribute significantly to the understanding of the complicated behaviors of fluids confined in nanopores.

Acknowledgment. This work was supported by the Program for New Century Excellent Talents in University (NCET), and the financial support of the National Natural Science Foundation of China (NSFC) (Nos. 20876007 and 20725622) is also greatly appreciated.

(1) Free Energy per Particle for the Attractive Interaction a_{att}.

The Helmholtz free energy per particle for the attractive interaction is given by

$$a_{att} = a_1 + a_2 + a_r \tag{29}$$

In terms of the packing factor $\eta = {}^1/_6\rho\pi d^3$, we introduce the convenient polynomials

$$L(t) = (1 + \eta/2)t + 1 + 2\eta \tag{30}$$

$$S(t) = (1 - \eta)^2 t^3 + 6\eta(1 - \eta)t^2 + 18\eta^2 t - 12\eta(1 + 2\eta) \tag{31}$$

and the rational function

$$Q(t) = \frac{S(t) + 12\eta L(t)e^{-t}}{(1 - \eta)^2 t^3} \tag{32}$$

In addition to the original LJ potential, $u^{LJ}(r)$, defined in eq 1 above, we introduce an auxiliary "two-Yukawa" form, namely

$$u^{TY}(r) = \begin{cases} \infty, & r < d \\ -k_1\varepsilon\dfrac{e^{-z_1(r-d)}}{r} + k_2\varepsilon\dfrac{e^{-z_2(r-d)}}{r}, & r > d \end{cases} \tag{33}$$

where $k_1 = k_0 e^{z_1(\sigma-d)}$, $k_2 = k_0 e^{z_2(\sigma-d)}$, $k_0 = 2.1714\sigma$, $z_1 = 2.9637/\sigma$, and $z_2 = 14.0167/\sigma$.

Then, we can define the pair correlation functions $g_0(r)$ and $g_1(r)$, which are most simply expressed in terms of their Laplace transforms as

$$G_0(s) = \int_0^\infty r g_0(r) e^{-sr}\, dr = \frac{L(sd)e^{-sd}}{(1 - \eta)^2 Q(sd) s^2} \tag{34}$$

$$G_1(s) = \int_0^\infty r g_1(r) e^{-sr}\, dr = \frac{\beta\varepsilon k_1 e^{-sd}}{(s + z_1)Q^2(sd)\, Q^2(z_1 d)} - \frac{\beta\varepsilon k_2 e^{-sd}}{(s + z_2)Q^2(sd)\, Q^2(z_2 d)} \tag{35}$$

From these expressions, we can derive

$$rg_0(r) = \sum_{n=0}^{\infty}(-12\eta)^n C(1, n+1, n+1, r-n-1) \tag{36}$$

$$rg_1(r) = \beta\varepsilon k_1 \frac{(1-\eta)^4}{Q^2(z_1)}\sum_{n=0}^{\infty}(1+n)(-12\eta)^n D(6, n, n+2, z_1, r-n-1) - \beta\varepsilon k_2 \frac{(1-\eta)^4}{Q^2(z_2)}\sum_{n=0}^{\infty}(1+n)\times (-12\eta)^n D(6, n, n+2, z_2, r-n-1) \tag{37}$$

with coefficients $C(n_1,n_2,n_3,r)$ and $D(n_1,n_2,n_3,z,r)$ defined by

$$C(n_1,n_2,n_3,r) = \begin{cases} \sum_{\alpha=0}^{2}\sum_{i=1}^{n_3}\frac{B(n_1,n_2,n_3,i,\alpha)}{(i-1)!}r^{i-1}e^{t_\alpha r}H(r), & n_1+n_2<3n_3 \\ \frac{(1+\eta/2)^{n_2}}{(1-\eta)^{2n_3}}\delta(r) + \sum_{\alpha=0}^{2}\sum_{i=1}^{n_3}\frac{B(n_1,n_2,n_3,i,\alpha)}{(i-1)!}r^{i-1}e^{t_\alpha r}H(r), & n_1+n_2=3n_3 \end{cases} \tag{38}$$

$$D(n_1,n_2,n_3,z,r) = \int_0^r C(n_1,n_2,n_3,y)e^{-z(r-y)}\,dy\,H(r) = \begin{cases} \sum_{\alpha=0}^{2}\sum_{i=1}^{n_3}\frac{(-1)^i B(n_1,n_2,n_3,i,\alpha)}{(t_\alpha+z)^i}\times \left[e^{-zr} - e^{t_\alpha r}\sum_{j=0}^{i-1}\frac{(-1)^j(t_\alpha+z)^j r^j}{j!}\right]H(r), & n_1+n_2<3n_3 \\ \frac{(1+\eta/2)^{n_2}}{(1-\eta)^{2n_3}}e^{-zr}H(r) + \sum_{\alpha=0}^{2}\sum_{i=1}^{n_3}\frac{(-1)^i B(n_1,n_2,n_3,i,\alpha)}{(t_\alpha+z)^i}\times \left[e^{-zr} - e^{t_\alpha r}\sum_{j=0}^{i-1}\frac{(-1)^j(t_\alpha+z)^j r^j}{j!}\right]H(r), & n_1+n_2=3n_3 \end{cases} \tag{39}$$

where $H(r)$ and $\delta(r)$ are the Heaviside step function and the Dirac delta function, respectively, while t_α ($\alpha = 0, 1, 2$) represents the roots of the equation $S(t) = 0$, and t_β and t_γ are the two zeros of $S(t)$ other than t_α when α is fixed.

The coefficients $B(n_1,n_2,n_3,i,\alpha)$ are, in turn, given by

$$B(n_1,n_2,n_3,i,\alpha) = \frac{1}{(1-\eta)^{2n_3}}\times \sum_{k_1=0}^{n_3-i}\sum_{k_2=0}^{n_3-i-k_1}\frac{(-1)^{n_3-i-k_1}(n_3-1+k_2)!(2n_3-1-i-k_1-k_2)!}{k_1!k_2!(n_3-1-k_1-k_2)![(n_3-1)!]^2}\times \frac{A(n_1,n_2,k_1,t_\alpha)}{(t_\alpha-t_\beta)^{n_3+k_2}(t_\alpha-t_\gamma)^{2n_3-i-k_1-k_2}} \tag{40}$$

with the coefficients $A(n_1,n_2,k_1,t_\alpha)$ defined as

$$A(n_1,n_2,k_1,t_\alpha) = \sum_{i=\max(k_1-n_1,0)}^{n_2}\frac{n_2!(i+n_1)!}{i!(n_2-i)!(i+n_1-k_1)!}\times (1+\eta/2)^i(1+2\eta)^{n_2-i}t_\alpha^{n_1+i-k_1} \tag{41}$$

Finally, we can express the various contributions to the attractive interaction term, including a_r, the revised part brought by the simplified exponential approximation, as

$$\begin{aligned} a_1 &= 2\pi\rho\beta\int_\sigma^\infty g_0(r)\,u(r)r^2\,dr \\ &= 2\pi\rho\beta\int_d^\infty [g_0(r)-1]u^{TY}(r)r^2\,dr + 2\pi\rho\beta\int_d^\infty u^{LJ}(r)r^2\,dr - 2\pi\rho\beta\int_d^\sigma g_0(r)\,u^{LJ}(r)r^2\,dr \\ &= -\frac{12\eta\beta\varepsilon}{d^3}\left\{k_1\left[\frac{L(z_1d)}{z_1^2(1-\eta)^2Q(z_1d)} - \frac{1+z_1d}{z_1^2}\right] - k_2\left[\frac{L(z_2d)}{z_2^2(1-\eta)^2Q(z_2d)} - \frac{1+z_2d}{z_2^2}\right]\right\} + 48\eta\beta\varepsilon\left[\frac{1}{9}\left(\frac{\sigma}{d}\right)^{12} - \frac{1}{3}\left(\frac{\sigma}{d}\right)^6\right] - 48\eta\beta\varepsilon\frac{1+\eta/2}{(1-\eta)^2}\left[\frac{1}{9}\left(\frac{\sigma}{d}\right)^{12} - \frac{1}{3}\left(\frac{\sigma}{d}\right)^6 + \frac{2}{9}\left(\frac{\sigma}{d}\right)^3\right] \end{aligned} \tag{42}$$

$$a_2 = \pi\rho\beta\int_\sigma^\infty g_1(r)\,u(r)r^2\,dr = \pi\rho\beta\int_d^\infty g_1(r)\,u^{TY}(r)r^2\,dr - \pi\rho\beta\int_d^\sigma g_1(r)\,u^{LJ}(r)r^2\,dr = -\frac{6\eta\beta^2\varepsilon^2}{d^3}\left[\frac{k_1^2}{2z_1Q^4(z_1d)} + \frac{k_2^2}{2z_2Q^4(z_2d)} - \frac{2k_1k_2}{(z_1+z_2)Q^2(z_1d)\,Q^2(z_2d)}\right] - 24\eta\beta^2\varepsilon^2\left[\frac{k_1/d}{Q^2(z_1d)} - \frac{k_2/d}{Q^2(z_2d)}\right]\left[\frac{1}{9}\left(\frac{\sigma}{d}\right)^{12} - \frac{1}{3}\left(\frac{\sigma}{d}\right)^6 + \frac{2}{9}\left(\frac{\sigma}{d}\right)^3\right] \tag{43}$$

$$a_r = 2\pi\rho\beta\int_\sigma^\infty g_0(r)\frac{e^{g_1(r)} - 1 - g_1(r) - g_1^2(r)/[2g_0(r)]}{g_1(r)}u^{LJ}(r)r^2\,dr \tag{44}$$

(2) DCF from the Attractive Contribution $c_{att}(r)$.

The DCF of bulk fluids from the attractive contribution is defined as

$$c_{att}(r) = c(r) - c_{hs}(r) \tag{45}$$

with the DCF of hard spheres, $c_{hs}(r)$, given by[45]

$$c_{hs}(r) = \begin{cases} -\frac{\eta(1+2\eta)^2}{2(1-\eta)^4}r^3 + \frac{6\eta(1+\eta+\eta^2/4)}{(1-\eta)^4}r - \frac{(1+2\eta)^2}{(1-\eta)^4}, & r<1 \\ 0, & r>1 \end{cases} \tag{46}$$

For a spherically symmetrical fluid, the total DCF, $c(r)$, relates to the total correlation function $h(r)$, or the RDF $g(r) = h(r) + 1$, through the OZ equation

$$\tilde{h}(k) = \tilde{c}(k) + \rho\tilde{h}(k)\,\tilde{c}(k) \tag{47}$$

where the tilde indicates the Fourier transform. Thus, to obtain accurate $\tilde{c}(k)$ or $c(r)$ expressions, we employ the exponent form of the RDF as input[30]

$$g(r) = g_0(r)\exp[g_1(r)] \tag{48}$$

where $g_0(r)$ and $g_1(r)$ are the same as in eqs 36 and 37, respectively.

References and Notes

(1) Chandler, D.; Oppenheim, I. *J. Chem. Phys.* **1968**, *49*, 2121.
(2) Evans, R. *J. Phys.: Condens. Matter* **1990**, *2*, 8989.
(3) Evans, R.; Marconi, U. M. B. *J. Chem. Phys.* **1987**, *86*, 7138.
(4) Tarazona, P.; Marconi, U. M. B.; Evans, R. *Mol. Phys.* **1987**, *60*, 573.
(5) Nakanishi, H.; Fisher, M. E. *J. Chem. Phys.* **1983**, *78*, 3279.
(6) Fisher, M. E.; Nakanishi, H. *J. Chem. Phys.* **1981**, *75*, 5857.
(7) Gelb, L. D.; Gubbins, K. E.; Radhakrishnan, R.; Sliwinska-Bratkowiak, M. *Rep. Prog. Phys.* **1999**, *62*, 1573.
(8) Ebner, C.; Saam, W. F. *Phys. Rev. Lett.* **1977**, *38*, 1486.
(9) Binder, K. In *Phase Transitions and Critical Phenomena*; Domb, C., Lebowitz, J. L., Eds.; Academic Press: London, 1983; Vol. 8, p 1.
(10) Privman, V. *Finite Size Scaling and Numerical Simulation*; World Scientific: Singapore, 1990.
(11) Diehl, H. W. *J. Phys.: Condens. Matter* **1998**, *2*, 9610143.
(12) Bykov, T. V.; Zeng, X. C. *J. Chem. Phys.* **2002**, *117*, 1851.
(13) Coasne, B.; Czwartos, J.; Sliwinska-Bratkowiak, M.; Gubbins, K. E. *J. Phys. Chem. B* **2009**, *113*, 13874.
(14) Nakanishi, H.; Fisher, M. E. *Phys. Rev. Lett.* **1982**, *49*, 1565.
(15) Drzewinski, A.; Maciolek, A.; Evans, R. *Phys. Rev. Lett.* **2000**, *85*, 3079.
(16) Binder, K.; Landau, D.; Muller, M. *J. Stat. Phys.* **2003**, *110*, 1411.
(17) Vishnyakov, A.; Piotrovskaya, E. M.; Brodskaya, E. N.; Votyakov, E. V.; Tovbin, Y. K. *Langmuir* **2001**, *17*, 4451.
(18) Radhakrishnan, R.; Gubbins, K. E.; Sliwinska-Bartkowiak, M. *J. Chem. Phys.* **2000**, *120*, 11048.
(19) Jiang, J.; Sandler, S. I.; Smit, B. *Nano Lett.* **2004**, *4*, 241.
(20) Hamada, Y.; Koga, K.; Tanaka, H. *J. Chem. Phys.* **2007**, *127*, 084908.
(21) Rosch, T. W.; Errington, J. R. *J. Phys. Chem. B* **2008**, *112*, 14911.
(22) Peng, B.; Yu, Y.-X. *J. Phys. Chem. B* **2008**, *112*, 15407.
(23) Neimark, A. V.; Lin, Y.; Ravikovitch, P. I.; Thommes, M. *Carbon* **2009**, *47*, 1617.
(24) Keshavarzi, E.; Kamalvand, M. *J. Phys. Chem. B* **2009**, *113*, 5493.
(25) Jagannathan, K.; Yethiraj, A. *Phys. Rev. Lett.* **2004**, *93*, 015701.
(26) Evenbly, G.; Vidal, G. *Phys. Rev. Lett.* **2009**, *102*, 180406.
(27) Berg, B. A.; Janke, W. *Phys. Rev. Lett.* **2007**, *98*, 040602.
(28) Wilson, K. G. *Phys. Rev. B* **1971**, *4*, 3174.
(29) Wilson, K. G. *Phys. Rev. B* **1971**, *4*, 3184.
(30) Zeng, M.; Tang, Y.; Mi, J.; Zhong, C. *J. Phys. Chem. C* **2009**, *113*, 17428.
(31) Mi, J.; Tang, Y.; Zhong, C.; Li, Y.-G. *J. Phys. Chem. B* **2005**, *109*, 20546.
(32) Mi, J.; Zhong, C.; Li, Y.-G.; Tang, Y. *AIChE J.* **2006**, *52*, 342.
(33) Yu, Y.-X.; Wu, J. *J. Chem. Phys.* **2002**, *117*, 10156.
(34) Tang, Y.; Lu, B. C.-Y. *Mol. Phys.* **1997**, *90*, 215.
(35) White, J. A.; Zhang, S. *J. Chem. Phys.* **1993**, *99*, 2012.
(36) Lue, L.; Prausnitz, J. M. *AIChE J.* **1998**, *44*, 1455.
(37) Young, T. *Philos. Trans. R. Soc. London* **1805**, *95*, 65.
(38) Nijmeijer, M. J. P.; Bruin, C.; Bakker, A. F.; van Leeuwen, J. M. J. *Phys. Rev. A* **1990**, *42*, 6052.
(39) He, Y.; Mi, J.; Zhong, C. *J. Phys. Chem. B* **2008**, *112*, 7251.
(40) Tang, Y. *J. Chem. Phys.* **2005**, *123*, 204704.
(41) Sadus, R. J. *High Pressure Phase of Behavior of Multicomponent Fluid Mixtures*; Elsevier: Amsterdam, 1992.
(42) Lotfi, A.; Vrabec, J.; Fischer, J. *Mol. Phys.* **1992**, *76*, 1319.
(43) Stanley, H. E. *Introduction to Phase Transitions and Critical Phenomena*; Oxford University Press: New York, 1987.
(44) Parry, A. O.; Evans, R. *Phys. Rev. Lett.* **1990**, *64*, 439.
(45) Thiele, E. *J. Chem. Phys.* **1963**, *39*, 474.

JP911070A